

**Deformational response of a marine silty-clay with varying organic content in the triaxial compression space.**

Ponzoni, Elisa; Muraro, Stefano; Nocilla, Alessandra; Jommi, Cristina

**DOI**

[10.1139/cgj-2023-0058](https://doi.org/10.1139/cgj-2023-0058)

**Publication date**

2023

**Document Version**

Accepted author manuscript

**Published in**

Canadian Geotechnical Journal

**Citation (APA)**

Ponzoni, E., Muraro, S., Nocilla, A., & Jommi, C. (2023). Deformational response of a marine silty-clay with varying organic content in the triaxial compression space. *Canadian Geotechnical Journal*. <https://doi.org/10.1139/cgj-2023-0058>

**Important note**

To cite this publication, please use the final published version (if applicable). Please check the document version above.

**Copyright**

Other than for strictly personal use, it is not permitted to download, forward or distribute the text or part of it, without the consent of the author(s) and/or copyright holder(s), unless the work is under an open content license such as Creative Commons.

**Takedown policy**

Please contact us and provide details if you believe this document breaches copyrights. We will remove access to the work immediately and investigate your claim.

***Green Open Access added to TU Delft Institutional Repository***

***'You share, we take care!' - Taverne project***

**<https://www.openaccess.nl/en/you-share-we-take-care>**

Otherwise as indicated in the copyright section: the publisher is the copyright holder of this work and the author uses the Dutch legislation to make this work public.

**Title:** Deformational response of a marine silty-clay with varying organic content in the triaxial compression space.

**Authors**

Elisa Ponzoni<sup>1</sup>

Stefano Muraro<sup>2</sup>

Alessandra Nocilla<sup>3</sup>

Cristina Jommi<sup>2,4</sup>

**Affiliation**

1 Rina S.p.A., Via Antonio Cecchi, 6, 16129 Genova, Italy

2 Department of Geoscience and Engineering, Delft University of Technology, Delft, The Netherlands

3 Department of Civil Engineering, Architecture, Environmental and Land Engineering, Università di Brescia, Brescia, Italy

4 Department of Civil and Environmental Engineering, Politecnico di Milano, piazza Leonardo da Vinci 32, 20133, Milano, Italy

**Correspondence to**

Stefano Muraro, Department of Geoscience and Engineering

Delft University of Technology, Stevinweg 1 / PO-box 5048, 2628 CN Delft / 2600 GA Delft, The Netherlands

e-mail: S.Muraro@tudelft.nl

1 **ABSTRACT**

2 This study characterises the effects of naturally varying organic content on the compression and shear  
3 behaviour of a marine silty-clay from the Netherlands. Index properties and mechanical properties are  
4 determined through laboratory tests, including oedometer and multistage loading-unloading triaxial stress  
5 paths. The results indicate a significant impact of the organic content on the compression response, with  
6 both the loading and reloading indexes increasing as the loss on ignition increases from 3% to 7%.  
7 Additionally, the study suggests a directional response of the compression behaviour, with the loading index  
8 increasing with the stress ratio. The influence of the organic content on shear strength appears to be less  
9 significant. No brittle response is observed during shearing and a similar ultimate stress ratio is attained by  
10 all samples. However, a unique critical state line can only be identified for samples with similar organic  
11 content, as its intercept and slope are found to increase with increasing organic content. The experimental  
12 results from stress paths at constant stress ratio reveal an anisotropic pre-failure plastic deformation mode,  
13 which depends on the previous stress history and loading direction. This suggests that the stress-dilatancy  
14 relationship cannot be formulated as a unique function of the stress ratio. The high-quality experimental  
15 data presented in the paper enlarge the database on soft organic soils in view of the development of  
16 advanced constitutive models.

17

18 **Keywords** Soft soils, Triaxial tests, Compression behaviour, Shear behaviour, Organic matter

19

20

## 21 INTRODUCTION

22 In the Netherlands, soft soils represent a large portion of natural geo-materials within the sub-surface and  
23 serve as foundation layers for a vast range of structures and infrastructure. Advanced characterisation of  
24 the geotechnical behaviour of soft soils is essential to support the development of constitutive models used  
25 more and more frequently in the assessment and design practice.

26  
27 In the past, extensive research focused on investigating the geotechnical behaviour of peat, which is  
28 traditionally considered the critical soil foundation layer for the stability of earth structures. Field tests on  
29 existing and trial embankments and extensive experimental laboratory tests have been performed on peat  
30 in the last decades (Den Haan and Kruse 2007; Zwanenburg et al. 2012; Zwanenburg and Jardine 2015;  
31 Muraro and Jommi 2021). A recent field test on a regional dyke at the Leendert de Boerspolder near Leiden  
32 shed light on the behaviour of the different soft soil foundation layers in the pre-failure and failure  
33 mechanism (Jommi et al. 2021; Muraro 2019). Contrarily to the common assumption of peat being the  
34 weak soil layer, the field test showed that the stiffer organic silty-clay underlying the foundation peat was  
35 the critical layer where failure was triggered. The interface between peat and silty-clay had also been  
36 identified as the weak soil surface by Hendry et al. (2013) in the analysis of the stability of railway  
37 embankments founded on peat. Despite the large body of experimental research on peat, to the authors'  
38 knowledge, a systematic characterisation of the geotechnical behaviour of Dutch organic clays is still  
39 lagging behind except for the Oostvaardersplassen clay (Tigchelaar et al. 2001; Den Haan 2003; Cheng et  
40 al. 2007).

41  
42 The geotechnical behaviour of these soils appears to be strongly influenced by the peculiar characteristic  
43 of their fabric, which often contains amorphous organic matter, fibres, stems, wood fragments and micro-  
44 organisms such as algae and plankton, together with silicate and calcium microfossils (e.g. Cheng et al.  
45 2004; Cheng et al. 2007). The extensive research conducted to characterise the compression and shear  
46 behaviour of similar soils from all over the world brought to a broad distinction between diatomaceous (e.g.  
47 Ariake clay, Hachirogata clay, Osaka Bay clay, Mexico City clay and Bogotá clay) and non- or slightly  
48 diatomaceous soft soils (e.g. Bothkennar clay, Pusan clay, Bangkok clay, Singapore clay,  
49 Oostvaardersplassen clay). The presence of diatom microfossils has been found to have a remarkable impact  
50 on the engineering behaviour of such soils. Due to their hollow skeleton and the entrapped water in their  
51 intraskeletal pore space, diatoms increase the Atterberg's limits and plasticity, void ratio, hydraulic  
52 conductivity and compressibility (Lo 1962; Mesri et al. 1975; Tanaka and Locat 1999; Diaz-Rodriguez et  
53 al. 1992; Caicedo et al. 2018). Besides the increase in soil compressibility, diatomaceous soils exhibit

54 exceptionally high friction angles due to the rough surface and interlocking of diatoms with the soil fabric  
55 (Shiwakoti et al. 2002).

56

57 For non-diatomaceous soils, the organic matter in the form of micro-organisms, fibres, stems, leaves and  
58 amorphous matter predominates in the engineering response. Residues of marine organisms (e.g. planktonic  
59 and benthic), such as in the soil matrix of Bothkennar clay, were found to have important effects on the soil  
60 plasticity and compressibility due to organic cement contributing to sustaining large soil aggregates or  
61 pellets (Hight et al. 1992; Paul and Barras 1999). However, following Hight et al. (1992), this micro-  
62 organism-related organic matter is unlikely to affect the shearing resistance. On the contrary, organic  
63 material of terrestrial plant origin significantly alters the shear strength of soil through reinforcing effects.  
64 The abundance of micro-fibres in the soil matrix increases significantly the soil friction angle. Friction  
65 angles even above 60° were reported by Larsson (1990) for Swedish organic clay and gyttja with micro-  
66 fibres in the soil matrix.

67

68 In the Netherlands, silty-clays are found including both diatoms and fibres from plant origin. Extensive  
69 characterisation can be found in the literature for the Oostvaardersplassen clay, where wood fragments,  
70 stems, rootlets and micro-fibres co-exist with micro-organisms such as algae and plankton, amorphous  
71 organics and silicate and calcium carbonate microfossils (Tigchelaar et al. 2001; Den Haan 2003). This  
72 work presents a systematic characterisation of an organic silty-clay found in the foundation of the full-scale  
73 test at Leendert de Boerspolder (Jommi et al. 2021). The soil is found in a marine prevalently silty parent  
74 area formed during the Holocene (de Bakker, 1979). Oedometer and multistage triaxial stress paths are  
75 conducted on undisturbed samples with varying organic content and diatomaceous inclusions. The pre-  
76 failure compression and shear response and strength are evaluated. The experimental data presented in this  
77 work improve existing datasets for the development of constitutive models for soft organic soils relevant  
78 to the engineering practice.

79

80

81

82

83

84

85

86

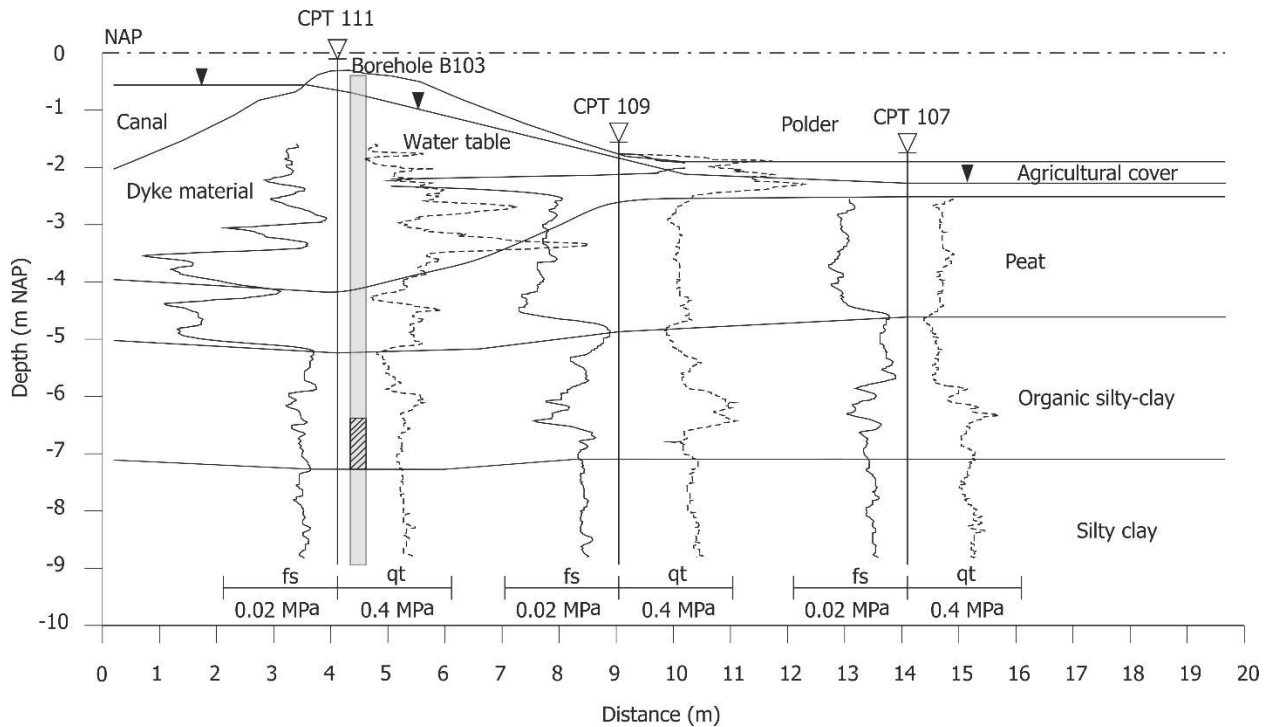
87

88 **EXPERIMENTAL PROGRAMME**

89 **Material and soil characterisation**

90 The soil used in this investigation was retrieved at the Leendert de Boerspolder site in the Netherlands. The  
91 soil profile is reported in Figure 1 and consists of: a) heterogeneous dyke material (i.e. silty sand with traces  
92 of gravel and clay, clayey silt with traces of sand); b) peat layer with a thickness between 1 m below the  
93 crest of the dyke and 2.5 m at the polder side; c) organic silty-clay deposit approximately 2 m thick  
94 characterised by variable organic content; d) thick deep silty-clay layer; and e) deep Pleistocene sand layer  
95 (not displayed in Figure 1). The Normaal Amsterdam Peil, NAP, is used as a reference system for elevation.  
96 The water level in the canal and the polder was regulated by the managing waterboard with small variations  
97 over time. The phreatic surface was located 0.3 m below the crest of the dyke at -0.6 m NAP. The dyke  
98 material was slightly overconsolidated (maximum OCR equal to 2.0) in the upper part while the OCR  
99 decreased with depth towards the normally consolidated state at the interface with the peat layer. The  
100 underlying peat layer and organic silty-clay were slightly overconsolidated or normally consolidated  
101 (Ponzoni 2017).

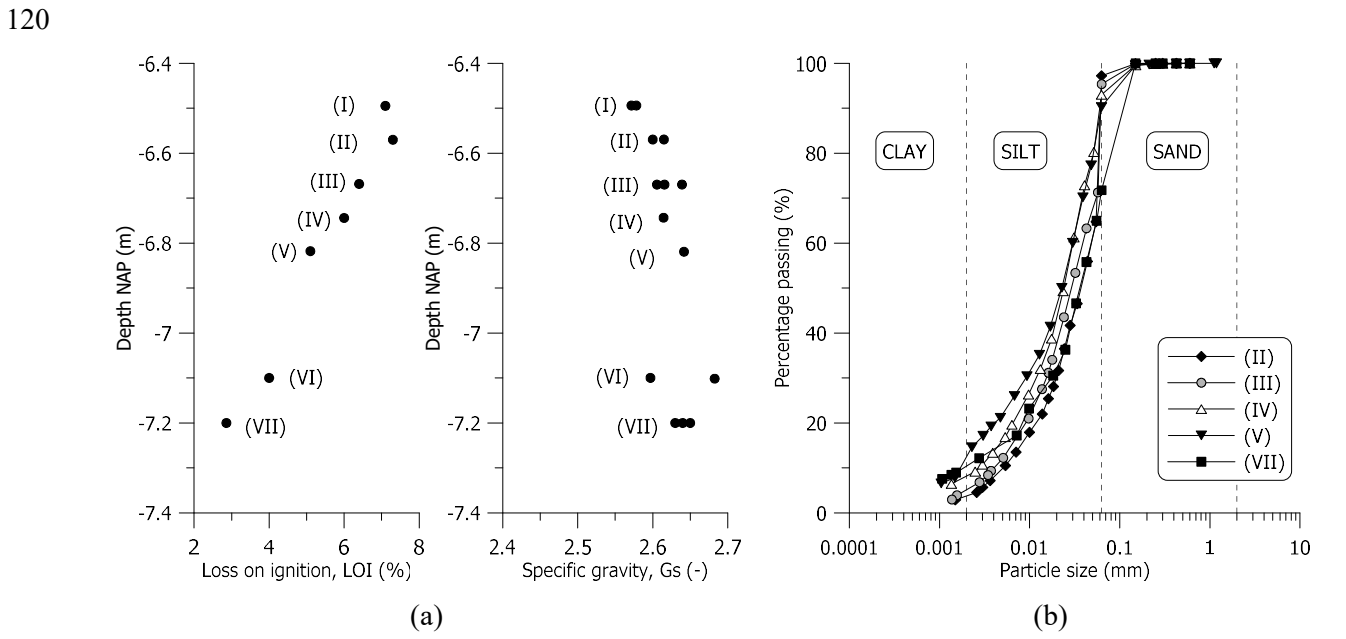
102 The experimental data presented in the following refer to the organic silty-clay soil layer. The samples were  
103 retrieved between -6.5 to -7.2 m NAP below the crest of the dyke using a 106 mm diameter piston sampler.  
104



105  
106  
107

Figure 1. Cross-section stratigraphy profile of the test site at the Leendert de Boerspolder

108 To reduce bio-degradation, the material was stored in a climate-controlled room at  $10 \pm 1^\circ\text{C}$  and 90%  
 109 relative humidity. To avoid loss of organic matter, the oven-drying procedures for soil classification were  
 110 performed at a temperature of  $60^\circ\text{C}$  (Head 2014). The specific gravity of the soil,  $G_s$ , was measured with a  
 111 helium pycnometer (D5550-14 2014). The loss on ignition, LOI, was determined by igniting oven-dried  
 112 samples in a furnace at  $440^\circ\text{C}$  (D2974-14 2014). The loss on ignition is used as a proxy of the variable  
 113 organic content over depth. The tested material was divided into seven groups based on the loss on ignition  
 114 as shown in Figure 2(a). The decrease of the LOI over depth from 7.3% to 2.9% is reflected in a general  
 115 increase in the specific gravity. Figure 2(b) reports the particle size distribution from wet-sieving and  
 116 hydrometer analysis for some of the tested groups (Head 2014; BS1377 1996). The soil composition ranges  
 117 from silt with traces of sand and clay to clayey sandy silt. The comparison in Figure 2 suggests that the  
 118 organic matter is mainly included in the silty fraction. The plastic and liquid limits range from  $w_p = 0.261$   
 119 to 0.408 and from  $w_l = 0.369$  to 0.774 with a LOI of 2.7% and 6.4%, respectively.



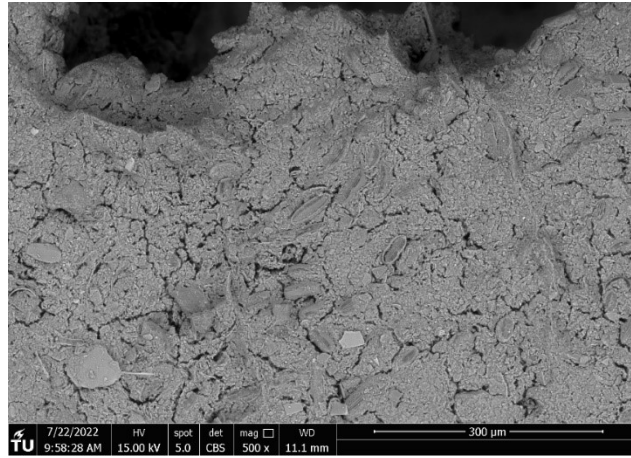
121 Figure 2. (a) Profile of loss on ignition and specific gravity; (b) particle size distributions of the tested  
 122 material

123  
 124 An impression of the fabric of the tested material is displayed in Figure 3 from three independent ESEM  
 125 (Environmental Scanning Electron Microscope) photomicrographs taken on natural samples with  
 126 LOI = 3 - 4%. The fabric is organised in aggregates with a characteristic size of 50 – 100  $\mu\text{m}$  where silty  
 127 particles, diatoms inclusions (Figure 3(a)), small wood fragments (Figure 3(b)), and pyrite framboids  
 128 (Figure 3(c)) are visible.

129



130  
131



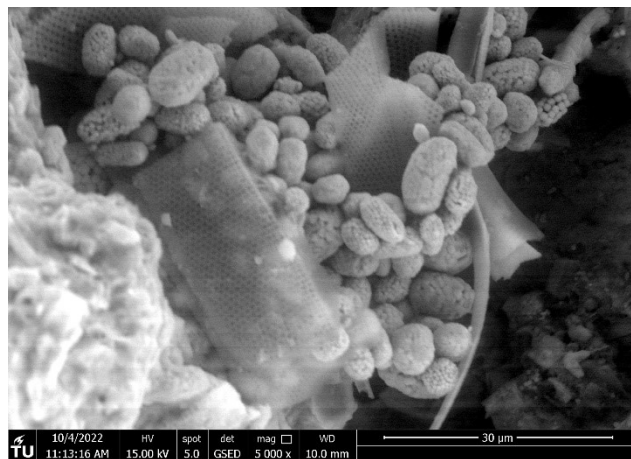
(a)

132  
133



(b)

134  
135



(c)

136 Figure 3. ESEM photomicrographs taken on independent soil samples at different magnification levels: (a)  
137 500x (LOI=4%), (b) 2000x (LOI=4%) and (c) 5000x (LOI=3%)

138 Relevant index properties of the samples are reported in Table 1, together with the initial void ratio of the  
 139 natural samples,  $e_i$ , the pre-consolidation mean effective stress applied in each test,  $p'_c$ , the mean effective  
 140 stress at the start of the shear,  $p'_s$ , and an indication of the stress path followed during each test. All the  
 141 samples were tested in undisturbed conditions except for one reconstituted sample, T2 (V), prepared with  
 142 a water content equal to the limit liquid (Burland 1990).

143  
 144

Table 1. Index properties, initial state and stress path of the tested specimens

Tube	Sample ID	Test	LOI (%)	Group	$e_i$ (-)	$p'_c$ (kPa)	$p'_s$ (kPa)
B103-13	T1	Oedometer	7.1	I	2.13	-	-
	T2	Oedometer	7.1		2.30	-	-
B103-13	T1	TxCU*	7.3	II	2.03	13	13
	T2	TxCU	7.3		2.00	25	25
	T3	TxCU	7.3		2.07	47	47
B103-13	T1	Isotropic	6.4	III	1.93	149	26
	T2	$K_0$ ***	6.4		1.93	-	11
	T3	Mixed****	6.4		1.82	67	36
B103-13	T1	Mixed	6.0	IV	1.78	64	36
	T2	Mixed	6.0		1.63	68	36
	T3	TxCU	6.0		1.79	80	80
B103-13	T1	Oedometer	5.1	V	1.55	-	-
	T2	Oedometer	5.7	V rec.	1.86	-	-
B103-14	T1	$p'$ constant	4.0	VI	1.27	14	14
	T2	TxCD**	4.0		1.31	14	14
B103-14	T1	Isotropic	2.9	VII	1.50	120	120
	T2	$K_0$	2.9		1.42	-	7

145 \*Undrained triaxial compression test, \*\*Drained triaxial compression test, \*\*\*  $K_0$  triaxial compression at null  
 146 lateral strain, \*\*\*\*Mixed: various combinations of stress paths at constant stress ratio,  $p'$  constant loading  
 147 unloading and  $q$  constant paths (see Figure 4 for the specific soil samples)

148

149 The nominal size of the tested specimens was 65 mm in diameter and 22 mm in height for incremental  
 150 loading oedometer tests and 38 mm in diameter and 76 mm in height for triaxial tests. The triaxial system  
 151 includes a submersible 1 kN load cell, a back pressure and cell pressure-volume controllers with an accuracy  
 152 of  $\pm 1$  kPa on pressure and  $\pm 300$  mm<sup>3</sup> on volume (0.15% full-scale range). A suction cap was used to

153 ensure perfect contact between the load cell and the top cap given the low effective confining stresses  
154 adopted in the experimental investigation. All the drained tests were performed under stress control assuring  
155 that the maximum excess pore pressure remained below 5% of the mean effective stress imposed on the  
156 samples.

157

### 158 **Stresses and strain variables**

159 The experimental data from triaxial tests are elaborated by assuming axisymmetric test conditions and  
160 adopting the common triaxial stress-strain variables: mean effective stress,  $p'$ , deviatoric stress,  $q$ ,  
161 volumetric strain,  $\varepsilon_p$ , and deviatoric strain,  $\varepsilon_q$ . Natural strains (Ludwik 1909) are adopted to elaborate the  
162 experimental data to avoid bias in the data interpretation due to the large displacements attained by the  
163 samples (Jommi et al. 2021)

164

$$\varepsilon_p = \varepsilon_a + 2\varepsilon_r = \ln\left(\frac{V_0}{V}\right) \quad (1)$$

165

$$\varepsilon_q = \varepsilon_a - \frac{\varepsilon_p}{3} = \ln\left(\frac{H_0}{H}\right) - \frac{1}{3}\ln\left(\frac{V_0}{V}\right) \quad (2)$$

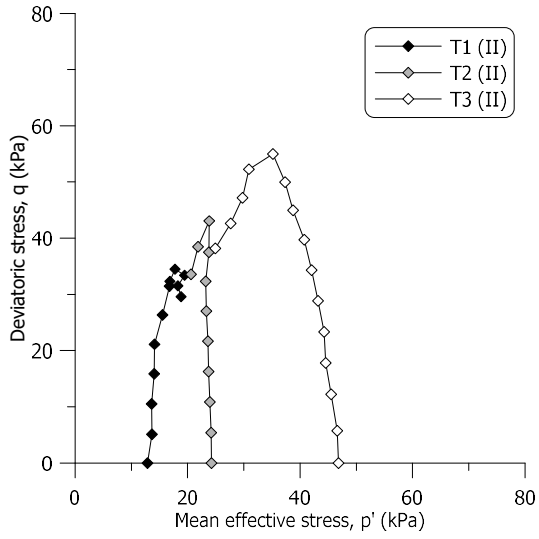
166

167 where  $V_0$  and  $H_0$  are the initial volume and height of the sample, respectively,  $V$  and  $H$  are the  
168 correspondent current values during the test,  $\varepsilon_a$  is the axial strain and  $\varepsilon_r$  is the radial strain. Compressive  
169 stresses and strains are assumed positive.

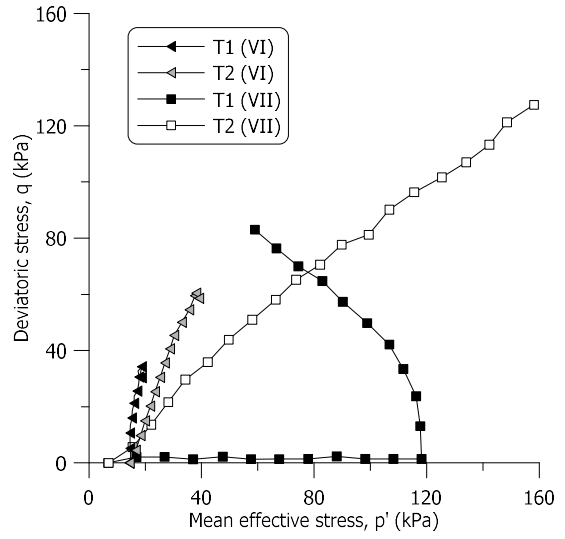
170

### 171 **Stress paths**

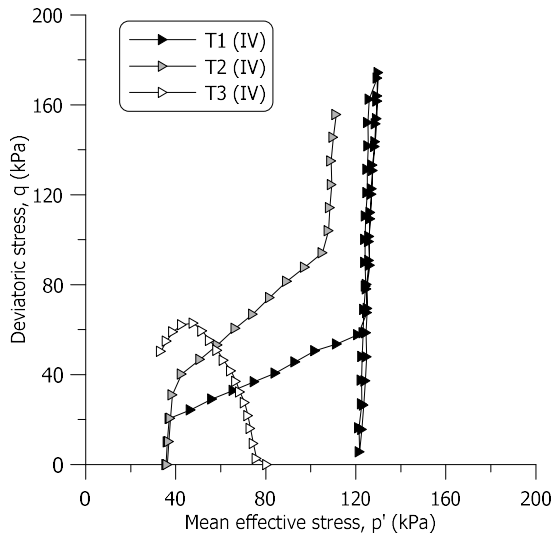
172 To investigate the volumetric behaviour, oedometer tests, isotropic and  $K_0$  compression tests were  
173 performed. The  $K_0$  compression tests were carried out in the triaxial apparatus with a radial stress ramp.  
174 Volume change and axial displacement back measurements allowed for automatic adjustment to guarantee  
175 negligible radial strains. Few samples were consolidated isotropically to  $p'_c$  to detect the initial yield  
176 surface. Afterwards, they were unloaded back to the isotropic stress  $p'_s$  indicated in Table 1. Eventually,  
177 the samples were sheared following different constraints (Figure 4). Samples from group (II) were brought  
178 to failure with standard TxCU tests (Figure 4(a)). Groups (VI) and (VII) were sheared following standard  
179 TxCU, TxCD and approximately constant  $p'$  after isotropic compression (Figure 4(b)). Multistage loading-  
180 unloading, compression at constant stress ratio, constant  $p'$  and constant  $q$  stress paths were followed on  
181 the samples of groups (III) and (IV), to better evaluate the non-monotonic pre-failure response (Figure 4(c),  
182 (d) and (e)).



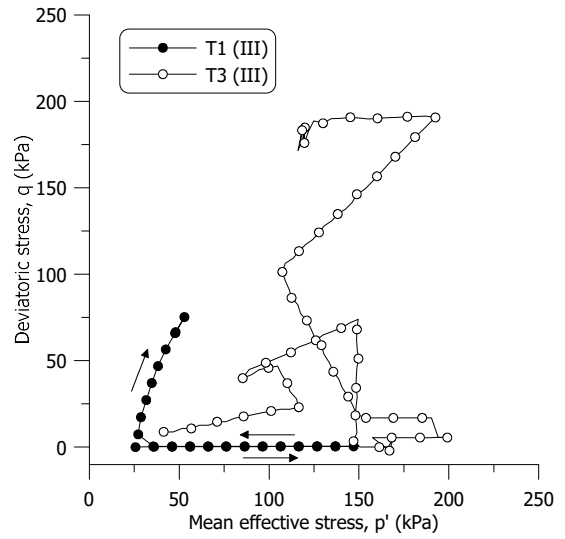
(a)



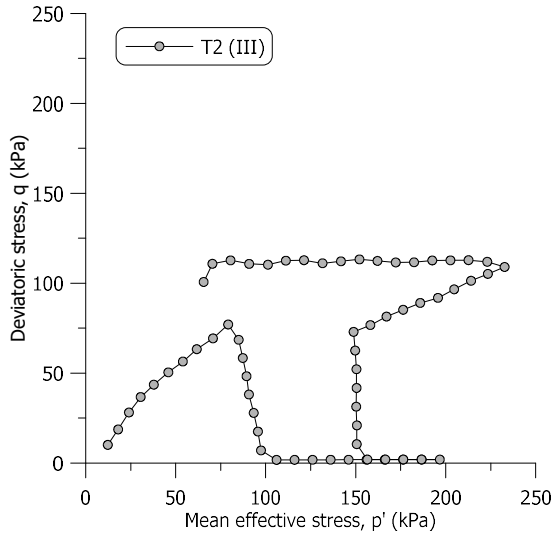
(b)



(c)



(d)



(e)

183 Figure 4. Experimental stress paths followed in the triaxial tests for groups of samples with different loss  
 184 on ignition: (a) group (II), (b) groups (VI) and (VII), (c) group (IV) and (d)-(e) group (III)  
 185

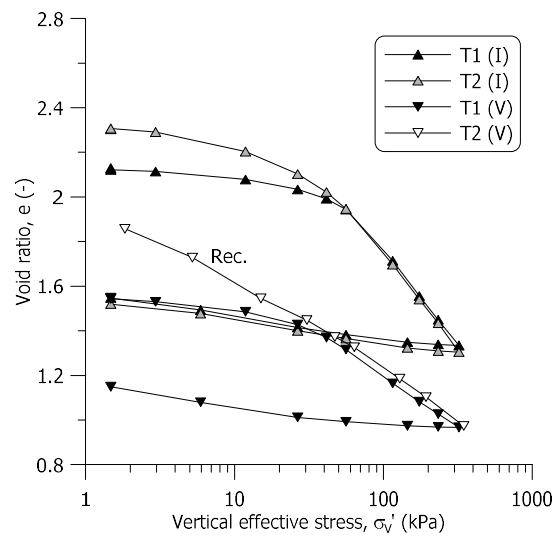
186 **EXPERIMENTAL RESULTS**

187

188 **Compression behaviour**

189 The oedometer tests performed on samples T1 (I), T2 (I) and T1 (V) allow identifying the effects of the  
190 organic matter on the compression behaviour as presented in Figure 5. A unique one-dimensional  
191 compression line, 1D-VCL, can be identified for each tested group. For group (I) with a LOI equal to 7.1%,  
192 the 1D-VCL has a slope  $C_c$  equal to 0.83 ( $\lambda \cong C_c/2.3 = 0.36$ ), whereas the inclination  $C_s$  of the unloading-  
193 reloading line (URL) has a value of 0.092 ( $\kappa \cong C_s/2.3 = 0.04$ ). For group (V) with a LOI of 5.1%,  
194  $C_c = 0.46$  ( $\lambda = 0.20$ ) and  $C_s = 0.05$  ( $\kappa = 0.022$ ) are found. The comparison between the natural T1 sample  
195 and reconstituted T2 sample from group (V) seems to suggest no significant destructuration effects for the  
196 tested material within the investigated stress range.

197



198

199 Figure 5. Oedometer curves for samples from groups (I) and (V)

200

201 The response upon isotropic and  $K_0$  compression in the triaxial tests on samples from group (III), LOI of  
202 6.4%, and group (VII) with the lowest LOI of 2.9% is shown in Figure 6. The slope of the ISO-NCL line  
203 decreases with the LOI from 0.32 to 0.16 and the slope of the  $K_0$  compression test (1D-VCL) from 0.36 to  
204 0.19. The slope of the unloading-reloading line from sample T1 (III) has a value of 0.036.

205

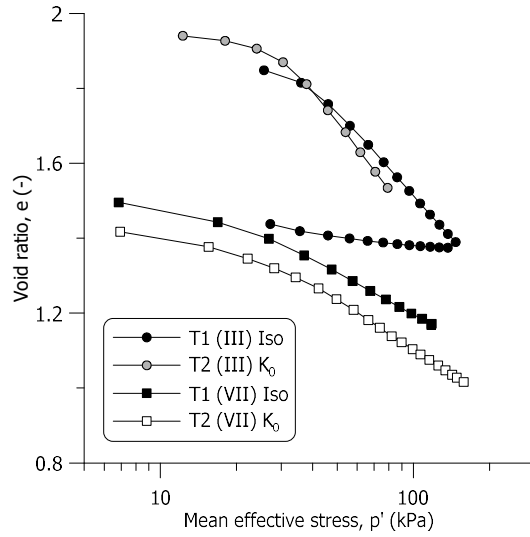
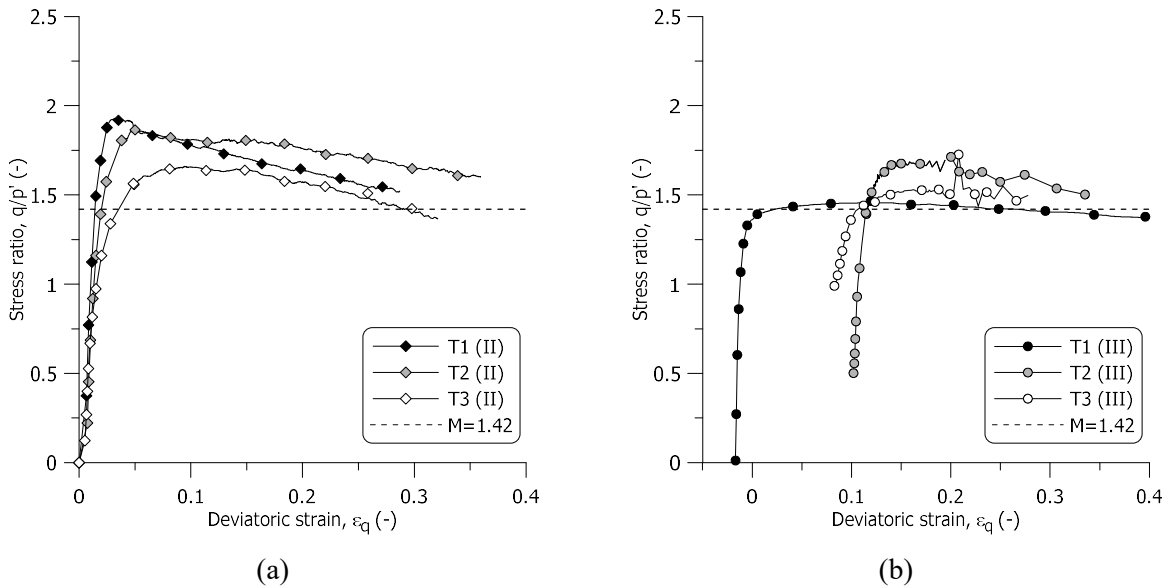


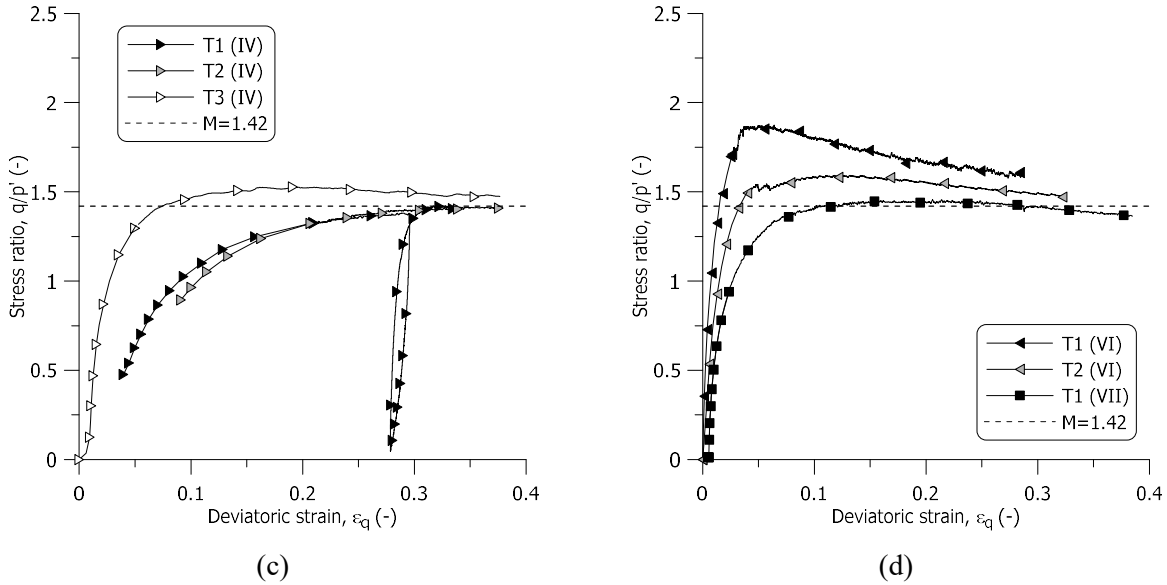
Figure 6. Isotropic and  $K_0$  compression data for samples from groups (III) and (VII)

206  
207  
208  
209  
210  
211  
212  
213

### Shear behaviour

The sample response upon shearing is summarised in Figure 7 in terms of stress ratio,  $q/p'$ , versus deviatoric strain for different groups of samples. For the sake of clarity, only the last portion of the stress path bringing each sample to failure is plotted.





214 Figure 7. Stress ratio versus deviatoric strain during the final shearing stage up to failure for groups of  
 215 samples with different loss on ignition: (a) group (II), (b) group (III), (c) group (IV), (d) groups (VI) and  
 216 (VII)

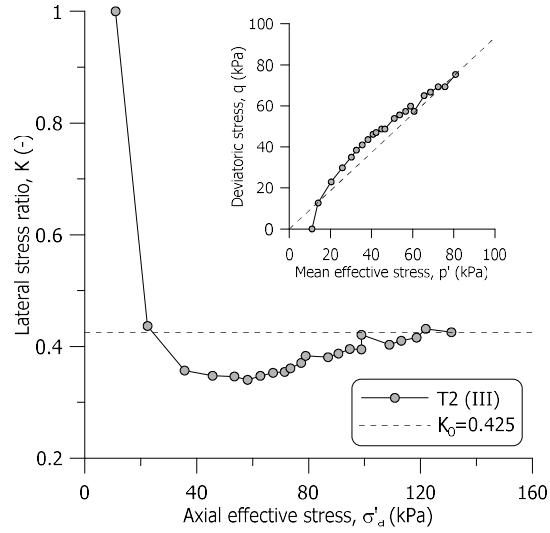
217  
 218

219 The results in Figure 7 suggest that the influence of the organic matter on the shear behaviour is less relevant  
 220 compared to what observed in the compression response. An ultimate stress ratio,  $M$ , equal to 1.42 ( $\varphi' = 35^\circ$ )  
 221 can be identified for almost all the sample groups. Only the samples from group (II) and group (VI) tested  
 222 at very low confining stresses,  $p' < 25$  kPa, attain a higher peak stress ratio equal to 1.8, followed by an  
 223 asymptotic decrease towards the ultimate stress ratio of 1.42. Small fluctuations in the peak stress ratio are  
 224 also found for samples T2 (III) and T3 (III) tested in stress-controlled unloading at constant deviatoric stress,  
 225 which results in poor controllability when the samples approach failure (Figure 4(b)). No significant brittle  
 226 response is observed upon shearing except for the overconsolidated samples T1 (II) and T2 (II), which  
 227 seems to confirm the absence of any significant destructuration for the tested material, as already anticipated  
 228 from the compression behaviour.

229

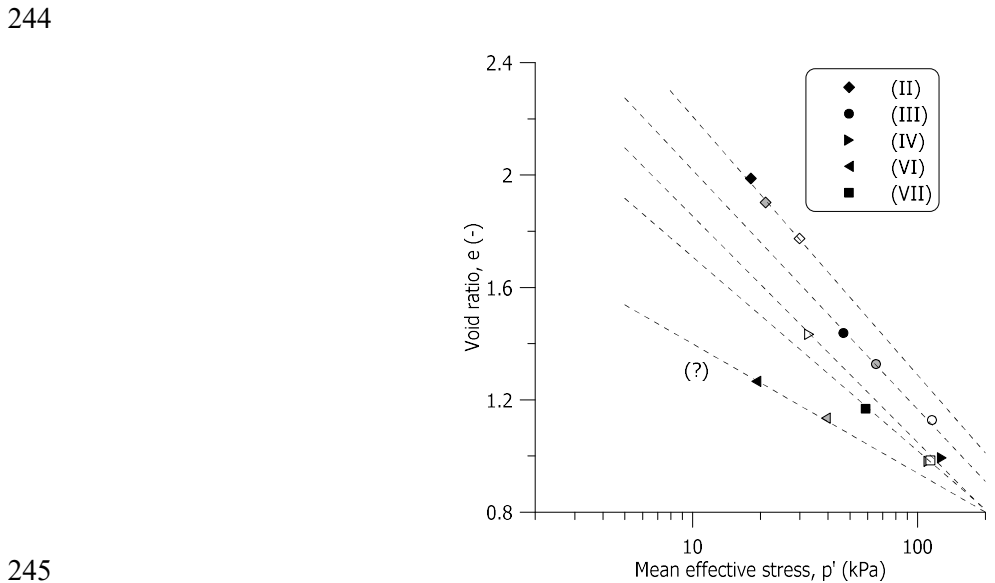
230 The ultimate friction angle  $\varphi' = 35^\circ$  gives a consistent estimate of the at-rest lateral earth pressure  
 231 coefficient in normally consolidated conditions using Jaky's simplified relationship ( $K_0 \cong 1 -$   
 232  $\sin \varphi' = 0.426$ ) compared to the experimental value,  $K_0 = 0.425$ , determined from sample T2 (III) (Figure  
 233 8). The value of  $K_0$  at normally consolidated state for the tested material agrees well with literature data on  
 234 various marine clays with similar plasticity index ( $0.20 < I_p < 0.40$ ) (Watabe et al. 2003).





235  
 236 Figure 8. Lateral stress ratio plotted against axial effective stress from the  $K_0$  compression test on sample  
 237 T2 (III)

238  
 239 The ultimate state attained by the different samples is presented in the  $e - p'$  space in Figure 9. The data  
 240 suggest that it is possible to identify a critical state line for samples belonging to the same group, within the  
 241 investigated stress level. The position of the critical state line (i.e. intercept,  $\Gamma$ ) and slope ( $\lambda$ ) are ruled by  
 242 the loss on ignition. As indicated in Figure 9, a general trend is observed with  $\Gamma$  and  $\lambda$  increasing with LOI  
 243 with the exception of the two samples from group (VI).



245  
 246 Figure 9. Ultimate state in the  $e - p'$  attained by samples from different groups after shearing

247  
 248

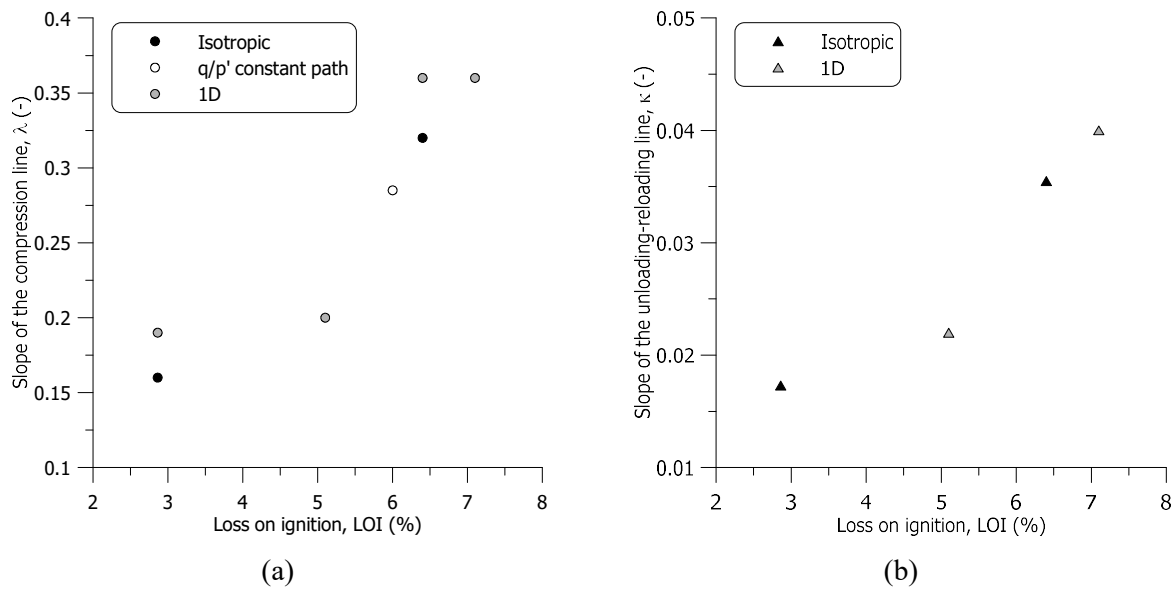
249 **DISCUSSION**

250

251 **Effects of organic matter and loading direction on the compression behaviour**

252 A comprehensive summary of the slope of the compression line and unloading-reloading line for samples  
253 with different LOI is presented in Figure 10, based on the different stress paths in Figure 4.

254



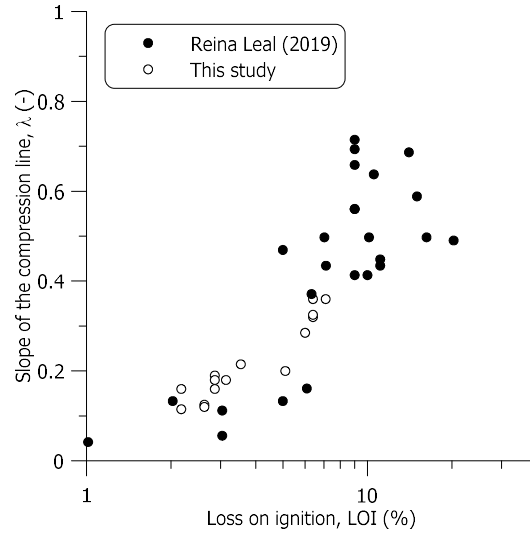
255 Figure 10. Dependence of the slope of the compression line (a) and unloading-reloading line (b) on the loss  
256 on ignition for different loading directions

257

258 The results confirm the significant role of the organic matter on the compression behaviour of the tested  
259 material. The slope of the compression line decreases from 0.360 to 0.160 for a LOI of 7.1% and 2.9%,  
260 respectively. The effect is also visible on the unloading-reloading line with a slope decreasing from 0.040  
261 to 0.017. The dependence of the compression response on the LOI found in Figure 10 aligns well with a  
262 large dataset of experimental results from oedometer tests on Bogotá clay samples encompassing a wide  
263 range of loss on ignition, displayed in Figure 11 (redrawn from Reina Leal 2019).

264

265



266  
 267 Figure 11. Variation of the slope of the compression line with the loss on ignition (redrawn from Reina Leal  
 268 2019)

269  
 270 Numerous correlations between the compression coefficient and index properties (e.g. liquid limit) have  
 271 been proposed in the literature for fine-grained materials (Balasubramaniam and Brenner 1981). Among  
 272 the proposals, the experimental data is compared in Figure 12a with the relationship proposed by Skempton  
 273 and Jones (1944) for remoulded clays and Terzaghi and Peck (1967) for normally consolidated clays. The  
 274 comparison shows that the tested material exhibits higher compressibility than that predicted by empirical  
 275 correlations on inorganic soils. The experimental data align well with the correlation proposed by Caicedo  
 276 et al. (2018) for Bogota' organic clays.

277 Noteworthy, the increase in the compressibility of the tested material is not associated with an increasing  
 278 percentage of clay fraction as commonly found for inorganic soils (Skempton and Jones 1944). On the  
 279 contrary, the compressibility is found to decrease with the clay fraction as displayed in Figure 12b. The  
 280 evidence is explained by the influence of the organic matter and diatoms on the soil compressibility, as  
 281 already noticed by Caicedo et al. (2018). Although both the LOI and the clay content contribute to the liquid  
 282 limit, the former predominates in the investigated material, as the positive correlation in Figure 10  
 283 demonstrates. This correlation allows inferring the compressibility of the tested soil from both:

284

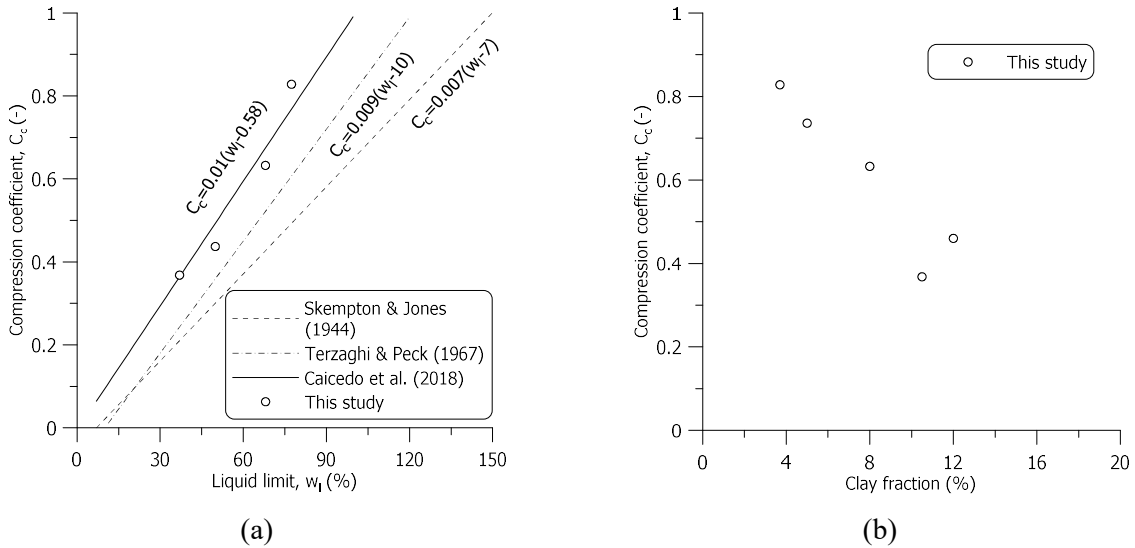
$$C_c = 0.01w_l \tag{3}$$

285 and

$$C_c = 0.07 + 0.11LOI \tag{4}$$

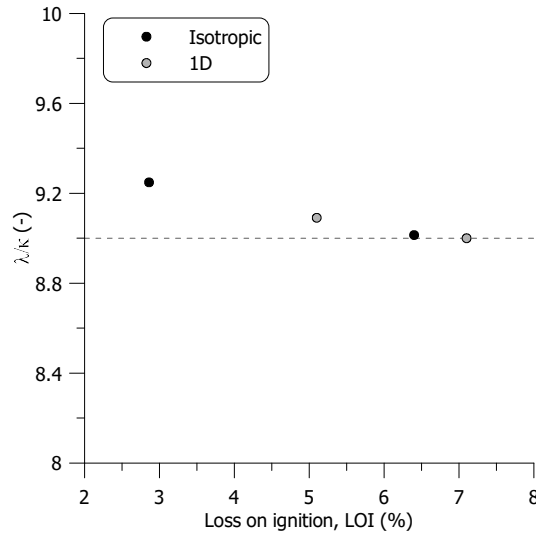
286

287 where  $w_l$  and LOI are expressed in percentages. Equation (4) is particularly useful in those countries where  
 288 organic soils are abundant and the LOI determination is included in the standard practice classification  
 289 procedure, more than Atterberg limits.  
 290



291 Figure 12. Correlation of the compression coefficient with liquid limit (a) and (b) clay fraction  
 292

293 The ratio  $\lambda/\kappa$  over different values of LOI is reported in Figure 13. The results show a slight tendency for  
 294 the  $\lambda/\kappa$  ratio to decrease with the organic matter, approaching a fairly constant value of 9 at increasing LOI.  
 295 A lower value for the  $\lambda/\kappa$  ratio of 7.6 is reported by Caicedo et al. (2018) for diatomaceous soil in lacustrine  
 296 deposits of Bogotá with a LOI ranging from 2% to 20%.  
 297

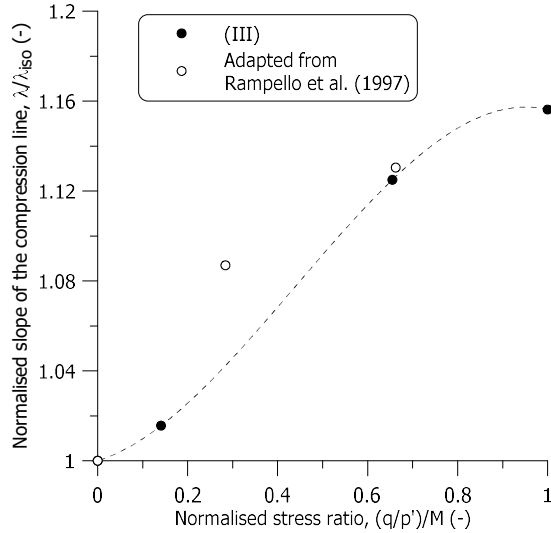


298  
 299 Figure 13. Influence of the loss on ignition on the ratio between the slope of the compression line and the  
 300 unloading-reloading line  
 301

302  
 303 The variation in the compression index shown in Figure 10 has been attributed primarily to the presence of  
 304 organic matter. It is worth noting that different diatoms content could also contribute to the observed  
 305 response. However, if the observed difference in compressibility were only due to a higher diatoms content,  
 306 differences in the shearing response among the different samples would also be expected. Shiwakoti et al.  
 307 (2002) tested artificial mixtures of Singapore clay and diatoms. For a diatom content increasing from 0%  
 308 to 40%, a 1.9-fold increase in the compression index,  $C_c$ , was observed, similar to the one in Figure 10a.  
 309 However, the increase in diatom content also led to a  $10^\circ$  increase in the ultimate friction angle, which was  
 310 not observed in our study (Figure 9). The evidence suggests that the difference in compressibility for the  
 311 tested material could be attributed primarily to variations in the micro-organisms-related organic matter.  
 312 Similar composition and fabric, including highly decomposed wood fragments, micro-organisms and  
 313 amorphous organic were found in the Oostvaardersplassen clay by Cheng et al. (2004) and Cheng et al.  
 314 (2007). The absence of significant differences in the ultimate friction angle within the investigated loss on  
 315 ignition also suggests that the decomposed plant fibres do not have a significant reinforcing effect contrary  
 316 to what is observed in fibrous soils. The organic matter of this type is hardly visible in ESEM, although it  
 317 was discovered by Tribovillard et al. (2022) inside pyrite framboids similar to the ones in Figure 3(c).  
 318

319 To broaden the view of the compression behaviour, the dependence of the compressibility on the loading  
 320 direction is investigated. To this aim, results on the volumetric response of samples from group (III) are  
 321 analysed including isotropic,  $K_0$  compression, and a stress path at a constant stress ratio  $q/p' = 0.2$ . The

322 slope of the compression line for each loading direction and of the critical state line normalised with the  
 323 one along isotropic loading ( $\lambda/\lambda_{iso}$ ) are compared in Figure 14.  
 324



325  
 326 Figure 14. Dependence of the slope of the compression line on the loading direction  
 327

328 The results show a dependence of the slope of the compression line on the loading direction, with  $\lambda$   
 329 increasing with the stress ratio. Similar evidence of the dependence of the slope of the normal compression  
 330 line on the stress path direction was also found by Rampello et al. (1997) on reconstituted samples of  
 331 Vallericca clay.

332  
 333

334 **Coupled deviatoric-volumetric deformation behaviour**

335 The pre-failure plastic deformation behaviour is analysed in terms of plastic strain increment vectors. The  
 336 post-yielding portions of the constant  $q/p'$  paths from groups (III) and (VII) (Figure 4) are considered. The  
 337 inclination of the plastic strain increment vectors,  $\beta$ , defined in equation (5) is plotted as a function of the  
 338 mean effective stress in Figure 15 for each test.

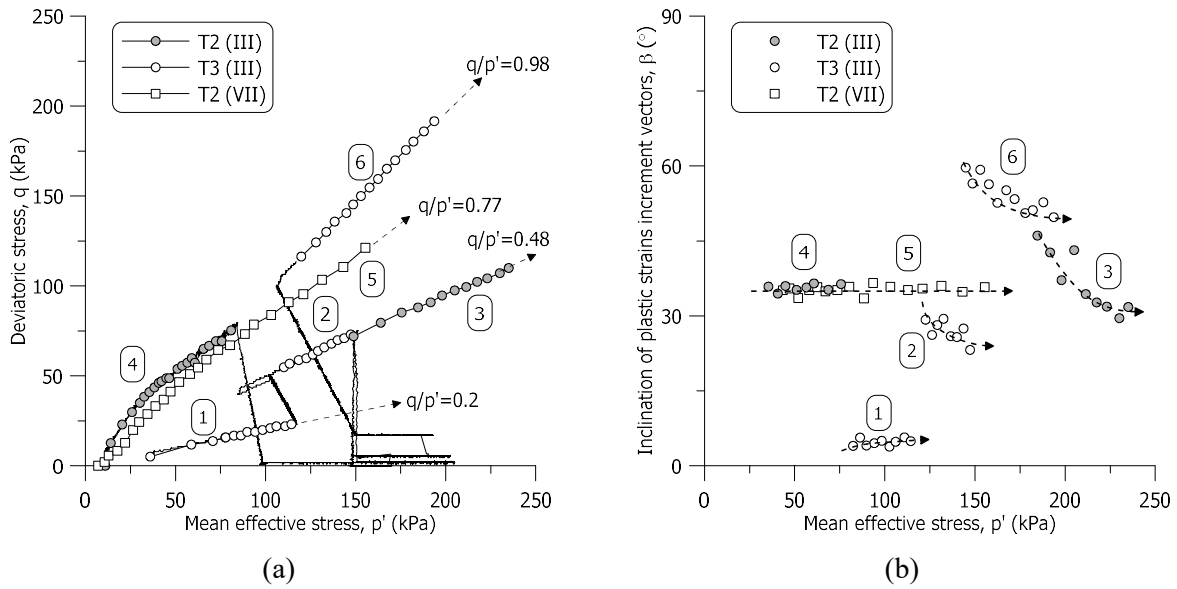
339

$$\tan \beta = \frac{\delta \epsilon_q^p}{\delta \epsilon_p^p} \quad (5)$$

340

341 The volumetric and the deviatoric plastic strain increments,  $\delta \epsilon_p^p$  and  $\delta \epsilon_q^p$ , have been derived from the total  
 342 ones by computing the elastic strains with a hypo-elastic isotropic law assuming a constant Poisson's ratio,

343  $\nu = 0.2$ . For each path, the value of  $\kappa$  has been determined either from the experimental data in Figure 10,  
 344 when available or computed from the polynomial interpolation in Figure 14, assuming an average  $\lambda/\kappa = 9.1$ .  
 345

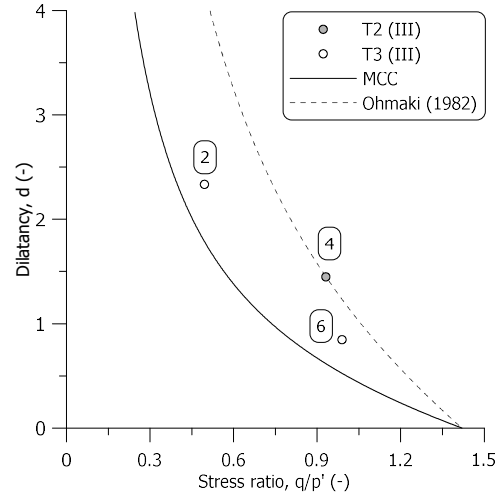


346 Figure 15. Stress paths (a) and (b) evolution of the inclination of the plastic strain increment vectors

347  
 348 The results in Figure 15(b) show an anisotropic plastic deformation behaviour. The plastic strain increment  
 349 vectors show a progressive rotation along the stress paths. The magnitude of the rotation seems to depend  
 350 on the previous stress history and the loading direction, as first suggested by Lewin and Burland (1970) and  
 351 Lewin (1973) in a study dedicated to the flow rule of clays. For the  $K_0$  compression tests on samples T2  
 352 (III) and T2 (VII), the plastic strain increment vectors do not rotate as a result of the initial alignment of the  
 353 fabric along the  $K_0$  line. On the contrary, along the subsequent path  $q/p' = 0.48$ , the plastic strain increment  
 354 vectors realign as a result of the difference between the current stress path and the previous stress history  
 355 of the sample (sample T2 (III) Figure 15(a)). For sample T3 (III), along the path  $q/p' = 0.2$  the rotation is  
 356 very limited due to the previous isotropic consolidation up to  $p'_c = 67$  kPa (Table 1), which realigned the  
 357 plastic strain increment vectors along the  $p'$ -axis. The magnitude of the rotation increases in the next paths  
 358 along  $q/p' = 0.48$  and  $q/p' = 0.98$ .

359  
 360 If the plastic strain increment vectors in Figure 15(b) are assumed to have reached the final inclination for  
 361 each constant  $q/p'$  stress path (i.e. saturation condition), they can be used to derive information on the  
 362 stress-dilatancy relationship. Figure 16 presents the dilatancy,  $d = 1/\tan \beta$ , derived from experimental  
 363 data of group (III), compared with common isotropic stress-dilatancy relationships.

364



365  
 366 Figure 16. Comparison between dilatancy from experimental results and common isotropic stress-dilatancy  
 367 relationships

368  
 369 The comparison with the  $K_0$  compression test (point 4 in Figure 16) confirms the well-known limitation of  
 370 the Modified Cam clay model, MCC, (Roscoe and Burland 1968) which tends to overestimate the  $K_0$  value  
 371 (Gens and Potts 1982; Alonso et al. 1990). To avoid this shortcoming, the expression of the stress-dilatancy  
 372 relationship of the MCC is often modified by means of a shape parameter  $\chi_g$  resulting in (Ohmaki 1982):  
 373

$$d = \frac{M^2 - \eta^2}{\chi_g \eta} \quad (6)$$

374  
 375 with  $\eta = q/p'$ . For  $\chi_g = 2$  the stress-dilatancy relationship of the MCC is recovered. The shape coefficient  
 376 in equation (6),  $\chi_g = 0.85$ , is calibrated on the  $K_0$  compression test. As shown in Figure 16, despite the  
 377 calibration of  $\chi_g$  to match the  $K_0$  path, the experimental dilatancy for the other constant  $q/p'$  stress paths  
 378 does not align with the new relationship. The experimental evidence suggests that the plastic deformation  
 379 mechanism changes with the loading direction and that the stress-dilatancy relationship cannot be  
 380 formulated as a unique function of the stress ratio,  $d = d(\eta)$ .

381  
 382  
 383 **CONCLUSIONS**

384  
 385 The laboratory characterisation of an organic silty-clay from the Netherlands is presented in this paper. The  
 386 material exhibits naturally varying organic content, with loss on ignition decreasing from 7% to 3% with  
 387 depth. The fabric is organised into aggregates with a characteristic size of 50-100  $\mu\text{m}$ , in which silty



388 particles, diatom inclusions, and small wood fragments are visible. Comparison between the particle size  
389 distribution across the samples suggests that the organic matter is mainly included in the silty fraction.  
390 Oedometer and triaxial compression tests indicate a dependence of the compressibility on the organic matter.  
391 The slope of the compression line,  $\lambda$ , and unloading reloading line,  $\kappa$ , decreases from 0.360 to 0.160 and  
392 from 0.040 to 0.017, respectively, across the range of loss on ignition investigated. The compressibility data  
393 also align with the relationship proposed by Caicedo et al. (2018) giving the compression coefficient as a  
394 function of the liquid limit. The  $\lambda/\kappa$  ratio slightly decreases at increasing organic matter, and levels off at  
395 a relatively constant value of 9.

396  
397 Compression tests along stress paths at constant stress ratio show a dependence of the slope of the  
398 compression line on the loading direction, with  $\lambda$  increasing with the stress ratio. Anisotropic post-yielding  
399 behaviour is observed where plastic strain increment vectors realign over stress paths at constant stress ratio.  
400 The magnitude of this realignment depends on the previous stress history and on the loading direction. The  
401 experimental evidence suggests that the stress-dilatancy relationship of this material cannot be formulated  
402 as a single function of the stress ratio.

403  
404 All the samples attain a similar ultimate stress ratio corresponding to a friction angle in triaxial compression  
405 of  $35^\circ$  regardless of the loss on ignition. This suggests that the effects of the organic matter on shear strength  
406 are less significant than on compression. However, the data show that a critical state line can only be  
407 identified for samples with similar organic content. A general trend is observed, with the intercept and slope  
408 of the critical state line increasing with the organic matter. The active  $K_0$  compression test in the triaxial  
409 apparatus shows that the critical state friction angle and the at-rest lateral earth pressure coefficient in  
410 normally consolidated conditions are well related by Jaky's simplified relationship. The response upon  
411 compression and the absence of significant post-failure brittleness during shear, seem to indicate that  
412 destructuration does not occur within the investigated stress range.

413  
414 The high-quality data presented in this study enrich the available database on soft silty-clays of marine  
415 origin containing non-fibrous organic matter and a moderate amount of diatoms. The data provide few hints  
416 on advanced modelling of the volumetric and deviatoric pre-failure behaviour of these soils.

#### 417 418 **ACKNOWLEDGMENT**

419 The financial support of the Dutch Organisation for Scientific Research (NWO), under the project  
420 "Reliability-Based Geomechanical Assessment Tools for Dykes and Embankments in Delta Areas - 13864  
421 (Reliable Dykes)" is gratefully acknowledged.

## REFERENCES

- Alonso, E.E., Gens, A., and Josa, A. 1990. A constitutive model for partially saturated soils. *Géotechnique*, **40**(3): 405-430. doi.org/10.1680/geot.1990.40.3.405.
- BS1377. 1996. Methods of test for Soils for civil engineering purposes Part 2. Classification tests. British Standard Institution, London.
- de Bakker, H. (1979). Major soils and soil regions in the Netherlands. W. Junk, B.V. Publishers, The Hague, the Netherlands.
- Balasubramaniam, A.S., and Brenner, R.P. 1981. Consolidation and settlement of soft clay. *In Soft Clay Engineering*. Brand and Brenner (eds), Amsterdam: Elsevier, pp. 481–566.
- Burland, J.B. 1990. On the compressibility and shear strength of natural clays. *Géotechnique*, **40**(3): 329-378. doi.org/10.1680/geot.1990.40.3.329.
- Caicedo, B., Mendoza, C., López, F., and Lizcano, A. 2018. Behavior of diatomaceous soil in lacustrine deposits of Bogotá, Colombia. *Journal of rock mechanics geotechnical engineering*, **10**(2): 367-379. doi.org/10.1016/j.jrmge.2017.10.005.
- Cheng, X.H., Ngan-Tillard, D.J.M., and Den Haan, E.J. 2007. The causes of the high friction angle of Dutch organic soils. *Engineering Geology*, **93**(1): 31-44. doi.org/10.1016/j.enggeo.2007.03.009.
- Cheng, X.H., Janssen, H., Barends, F.B.J., and Den Haan, E.J. 2004. A combination of ESEM, EDX and XRD studies on the fabric of Dutch organic clay from Oostvaardersplassen (Netherlands) and its geotechnical implications. *Applied Clay Science*, **25**(3-4): 179-185. doi.org/10.1016/j.clay.2003.11.002.
- D2974-14, A. 2014. Standard test methods for moisture, ash, and organic matter of peat and other organic soils. American Society of Testing and Materials.
- D5550-14, A. 2014. Standard test method for specific gravity of soil solids by gas pycnometer. American Society of Testing and Materials.
- Den Haan, E.J. 2003. Sample disturbance of soft organic Oostvaardersplassen clay. *Deformation Characteristics of Geomaterials*, Di Benedetto et al. (eds), 2003, 49-55.

- Den Haan, E.J., and Kruse, G.A.M. 2007. Characterisation and engineering properties of Dutch peats. *In* Proceedings of the Second International Workshop of Characterisation and Engineering Properties of Natural Soils. Singapore 2007. Tan and Phoon and Hight and Leroueil (eds). Taylor & Francis Group, pp. 2101-2133.
- Diaz-Rodriguez, J.A., Leroueil, S., and Aleman, J.D. 1992. Yielding of Mexico City clay and other natural clays. *Journal of Geotechnical Engineering*, **118**(7): 981-995. doi.org/10.1061/(ASCE)0733-9410(1992)118:7(981).
- Gens, A., and Potts, D.M. 1982. A theoretical model for describing the behaviour of soils not obeying Rendulic's principle. *In* Proceedings of the International Symposium on Numerical Models in Geomechanics. Zurich, Switzerland 1982, pp. 24-32.
- Head, K.H. 2014. Manual of soil laboratory testing – Vol. I: Soil classification and compaction tests. Whitteles Publishing, Dunbeath, UK.
- Hendry, M.T., Martin, C.D., and Barbour, S. 2013. Measurement of cyclic response of railway embankments and underlying soft peat foundations to heavy axle loads. *Canadian Geotechnical Journal*, **50**(5): 467-480. doi.org/10.1139/cgj-2012-0118.
- Hight, D.W., Bond, A.J., and Legge, J.D. 1992. Characterization of the Bothkennar clay: an overview. *Géotechnique*, **42**(2): 303-347. doi.org/10.1680/geot.1992.42.2.303.
- Jommi, C., Chao, C.Y., Muraro, S., and Zhao, H.F. 2021. Developing a constitutive approach for peats from laboratory data. *Geomechanics for Energy and the Environment*, **27**: 100220. doi.org/10.1016/j.gete.2020.100220.
- Larsson, R. 1990. Behaviour of organic clay and gyttja. Swedish Geotechnical Institute, Linköping, **38**.
- Leal Reina, R.C. 2019. Influencia del contenido de Materia Orgánica en el cambio volumétrico de arcillas blandas. MSc thesis, Universidad Nacional de Colombia, Bogotá, Colombia.
- Lewin, P.I. The influence of stress history on the plastic potential. *In* Proceedings of the Symposium on the Role of Plasticity in Soil Mechanics. Cambridge, England 1973, pp. 96-105.
- Lewin, P.I., and Burland, J.B. 1970. Stress-probe experiments on saturated normally consolidated clay. *Géotechnique*, **20**(1): 38-56. doi.org/10.1680/geot.1970.20.1.38.
- Lo, K.Y. 1962. Shear strength properties of a sample of volcanic material of the Valley of Mexico. *Géotechnique*, **12**(4): 303-318. doi.org/10.1680/geot.1962.12.4.303.

- Ludwik, P. 1909. *Elemente der technologischen Mechanik*. Springer-Verlag.
- Mesri, G., Rokhsar, A., and Bohor, B.F. 1975. Composition and compressibility of typical samples of Mexico City clay. *Géotechnique*, **25**(3): 527-554. doi.org/10.1680/geot.1975.25.3.527.
- Muraro, S. 2019. The deviatoric behaviour of peat: a route between past empiricism and future perspectives. PhD thesis, Delft University of Technology, Delft, the Netherlands.
- Muraro, S., and Jommi, C. 2021. Experimental determination of shear strength of peat from standard undrained triaxial tests: correcting for the effects of end restraint. *Géotechnique*, **71**(1): 76-87. doi.org/10.1680/jgeot.18.P.346.
- Ohmaki, S. 1982. Stress-strain behaviour of anisotropically, normally consolidated cohesive soil. *In* Proceeding 1st International Symposium on Numerical Models in Geomechanics. Zurich, Switzerland 1982, pp. 250-269.
- Paul, M.A., and Barras, B.F. 1999. Role of organic material in the plasticity of Bothkennar clay. *Géotechnique*, **49**(4): 529-535. doi.org/10.1680/geot.1999.49.4.529.
- Ponzoni, E. 2017. Historical constructions on natural silty soils accounting for the interaction with the atmosphere. PhD thesis, Università degli studi di Brescia, Brescia, Italy.
- Rampello, S., Viggiani, G.M.B., and Amorosi, A. 1997. Small-strain stiffness of reconstituted clay compressed along constant triaxial effective stress ratio paths. *Géotechnique*, **47**(3): 475-489. doi.org/10.1680/geot.1997.47.3.475.
- Roscoe, K.H., and Burland, J.B. 1968. On the generalized stress-strain behaviour of wet clay. *In* Engineering plasticity. *Edited by* Heyman and Leckie. Cambridge University Press, Cambridge, pp. 535–609.
- Shiwakoti, D.R., Tanaka, H., Tanaka, M., and Locat, J. 2002. Influences of diatom microfossils on engineering properties of soils. *Soils and foundations*, **42**(3): 1-17. doi.org/10.3208/sandf.42.3\_1.
- Skempton, A.W., and Jones, O.T. 1944. Notes on the compressibility of clays. *Quarterly Journal of the Geological Society*, **100**(1-4): 119-135. doi.org/10.1144/GSL.JGS.1944.100.01-04.08.
- Tanaka, H., and Locat, J. 1999. A microstructural investigation of Osaka Bay clay: the impact of microfossils on its mechanical behaviour. *Canadian Geotechnical Journal*, **36**(3): 493-508. doi.org/10.1139/t99-009.

- Terzaghi, K., and Peck, R.B. 1967. Soil mechanics in engineering practice. Wiley, New York.
- Tigchelaar, J., De Feijter, J.W., and Den Haan, E.J. 2001. Shear tests on reconstituted Oostvaardersplassen clay. *In* *Soft Ground Technology*, pp. 67-81.
- Tribovillard, N., Bout-Roumazeilles, V., Delattre, M., Ventalon, S., and Bensadok, A. 2022. Sedimentary pyrite as a trap of organic matter: preliminary results from large-framboid observation. *European Journal of Mineralogy*, **34**(1): 77-83. doi.org/10.5194/ejm-34-77-2022.
- Watabe, Y., Tanaka, M., Tanaka, H., and Tsuchida, T. 2003. K<sub>0</sub>-consolidation in a triaxial cell and evaluation of in-situ K<sub>0</sub> for marine clays with various characteristics. *Soils and foundations*, **43**(1): 1-20. doi.org/10.3208/sandf.43.1.
- Zwanenburg, C., and Jardine, R.J. 2015. Laboratory, in situ and full-scale load tests to assess flood embankment stability on peat. *Géotechnique*, **65**(4): 309-326. doi.org/10.1680/geot.14.P.257.
- Zwanenburg, C., Den Haan, E.J., Kruse, G.A.M., and Koelewijn, A.R. 2012. Failure of a trial embankment on peat in Booneschans, the Netherlands. *Géotechnique*, **62**(6): 479-490. doi.org/10.1680/geot.9.P.094.

## LIST OF SYMBOLS

$G_s$	specific gravity
LOI	loss on ignition
$e$	void ratio
$e_i$	initial void ratio
$\varepsilon_a$	axial strain
$\varepsilon_r$	radial strain
$\varepsilon_p$	volumetric strain
$\varepsilon_q$	deviatoric strain
$\nu$	Poisson's ratio
$H_0$	initial sample height
$V_0$	initial sample volume
$H$	current sample height
$V$	current sample volume
$w_p$	plastic limit
$w_l$	liquid limit
$I_p$	plasticity index
$C_c$	compression coefficient
$C_s$	unloading-reloading coefficient
$\lambda$	slope of the compression line
$\lambda_{iso}$	slope of the isotropic compression line
$\kappa$	slope of the unloading-reloading line
OCR	overconsolidation ratio
$\sigma'_v$	vertical effective stress

$\sigma'_a$	axial effective stress
$p'$	mean effective stress
$q$	deviatoric stress
$K$	lateral stress ratio
$K_0$	coefficient of earth pressure at rest
$\eta$	stress ratio
$M$	ultimate stress ratio
$\varphi'$	friction angle
$p'_c$	pre-consolidation mean effective stress
$p'_s$	mean effective stress at the start of the shear
$\Gamma$	intercept of the critical state line
$d$	dilatancy
$\chi_g$	shape parameter for the stress-dilatancy relationship
$\delta\varepsilon_p^p$	volumetric plastic strain increment
$\delta\varepsilon_q^p$	deviatoric plastic strain increment
$\beta$	inclination of the plastic strain increment vectors
$q_t$	corrected cone resistance
$f_s$	sleeve friction

## LIST OF FIGURES

Figure 1. Cross-section stratigraphy profile of the test site at the Leendert de Boerspolder

Figure 2. (a) Profile of loss on ignition and specific gravity; (b) particle size distributions of the tested material

Figure 3. ESEM photomicrographs taken on independent soil samples at different magnification levels: (a) 500x (LOI=4%), (b) 2000x (LOI=4%) and (c) 5000x (LOI=3%)

Figure 4. Experimental stress paths followed in the triaxial tests for groups of samples with different loss on ignition: (a) group (II), (b) groups (VI) and (VII), (c) group (IV) and (d)-(e) group (III)

Figure 5. Oedometer curves for samples from groups (I) and (V)

Figure 6. Isotropic and  $K_0$  compression data for samples from groups (III) and (VII)

Figure 7. Stress ratio versus deviatoric strain during the final shearing stage up to failure for groups of samples with different loss on ignition: (a) group (II), (b) group (III), (c) group (IV), (d) groups (VI) and (VII)

Figure 8. Lateral stress ratio plotted against axial effective stress from the  $K_0$  compression test on sample T2 (III)

Figure 9. Ultimate state in the  $e - p'$  attained by samples from different groups after shearing

Figure 10. Dependence of the slope of the compression line (a) and unloading-reloading line (b) on the loss on ignition for different loading directions

Figure 11. Variation of the slope of the compression line with the loss on ignition (redrawn from Reina Leal 2019)

Figure 12. Correlation of the compression index with the liquid limit (a) and (b) the clay fraction



Figure 13. Influence of the loss on ignition on the ratio between the slope of the compression line and the unloading-reloading line

Figure 14. Dependence of the slope of the compression line on the loading direction

Figure 15. Stress paths (a) and (b) evolution of the inclination of the plastic strain increment vectors

Figure 16. Comparison between dilatancy from experimental results and common isotropic stress-dilatancy relationships

## **LIST OF TABLES**

Table 1. Index properties, initial state and stress path of the tested specimens

**Competing interests**

The authors declare there are no competing interests.

**Data availability**

Data available upon request: data generated or analysed during this study are available from the corresponding author upon motivated request.